Detailing organelle division and segregation in *Plasmodium falciparum*

Julie M.J. Verhoef[1], Cas Boshoven[1], Felix Evers[1], Laura J. Akkerman[1], Barend C.A. Gijsbrechts[1], Marga van de Vegte-Bolmer[1], Geert-Jan van Gemert[1], Akhil B. Vaidya[2], Taco W.A. Kooij[1*]

[1]Department of Medical Microbiology, Radboudumc Center for Infectious Diseases, Radboud University Medical Center, Nijmegen, The Netherlands
[2]Center for Molecular Parasitology, Institute for Molecular Medicine and Infectious Disease, Department of Microbiology and Immunology, Drexel University College of Medicine, Philadelphia, USA

*Corresponding author: Taco.Kooij@radboudumc.nl

Abstract

The malaria causing parasite, *Plasmodium falciparum*, replicates through a tightly orchestrated process termed schizogony, where approximately 32 daughter parasites are formed in a single infected red blood cell and thousands of daughter cells in mosquito or liver stages. One-per-cell organelles, such as the mitochondrion and apicoplast, need to be properly divided and segregated to ensure a complete set of organelles per daughter parasites. Although this is highly essential, details about the processes and mechanisms involved remain unknown. We developed a new reporter parasite line that allows visualization of the mitochondrion in blood and mosquito stages. Using high-resolution 3D-imaging, we found that the mitochondrion orients in a cartwheel structure, prior to stepwise, non-geometric division during the last stage of schizogony. Analysis of focused ion beam scanning electron microscopy (FIB-SEM) data confirmed these mitochondrial division stages. Furthermore, these data allowed us to elucidate apicoplast division steps, highlighted its close association with the mitochondrion, and showed putative roles of the centriolar plaques (CPs) in apicoplast segregation. These observations form the foundation for a new detailed mechanistic model of mitochondrial and apicoplast division and segregation during *P. falciparum* schizogony and pave the way for future studies into the proteins and protein complexes involved in organelle division and segregation.

Introduction

Malaria is a devastating parasitic disease causing an estimated 249 million cases resulting in approximately 608,000 deaths in 2022, especially in children under 5 years old[1]. *Plasmodium falciparum* is the most virulent parasite species causing malaria. Continued emergence of resistant parasites to antimalarial drugs is a major problem for global malaria control and necessitates continued development of novel antimalarials.

The malaria parasite harbors a unique mitochondrion that differs greatly from the human mitochondrion at a molecular and functional level[2]. While the most prominent role of the mitochondrion in humans is respiration and consequent energy conversion, in the disease-causing asexual blood stages of *P. falciparum* the respiratory chain appears to be exclusively essential to support pyrimidine biosynthesis[3]. It is only during preparation for transition to the mosquito vector where sexual reproduction takes place, that canonical mitochondrial functions such as the tricarboxylic acid cycle (TCA) cycle and the oxidative phosphorylation (OXPHOS) pathway become more abundant and critical[4,5]. Because of these differences, it is not surprising that this organelle is the drug target of several anti-malarial compounds, such as atovaquone, DSM265, proguanil and ELQ300[6,7].

Host and stage transitions are commonplace in the complicated life cycle of *Plasmodium* parasites. During erythrocytic asexual replication, one parasite is segmented into approximately 32 merozoites through a tightly orchestrated process called schizogony. Cell division happens on a much larger scale in mosquito and liver stages, where one parasite is divided into thousands or even tens of thousands of daughter parasites. During *P. falciparum* cell division, the single parasite mitochondrion needs to be properly divided and distributed among the daughter cells[9]. During parasite development in asexual blood stages, the tubular mitochondrion elongates and forms a large, branched network that stretches throughout the parasite[10]. Only during the final stages of schizogony, once nuclear division is completed, does the mitochondrion undergo rapid fission[11]. The apicoplast, another essential single copy organelle of secondary endosymbiotic origin, forms a comparable branched network, but divides prior to mitochondrial fission during blood- and liver-stage replication[10,12]. To produce viable offspring, the parasite has to ensure that each daughter parasite has a complete set of these organelles. However, so far a detailed view of these processes and the mechanisms involved is lacking.

We aimed to capture the process of mitochondrial division in these multinucleated cells in detail using different imaging methods. However, this comes with several challenges. Firstly, imaging the small-sized parasites (1-7 μm diameter), and the even smaller organelles within the parasites, requires the use of super-resolution imaging techniques. Secondly, visualization of the mitochondrion requires a specific fluorescent marker or dye. Mitochondrial dyes, such as Rhodamine123 and MitoTracker™, have been widely used in the field[13]. These dyes rely on membrane potential to enter the mitochondrion and are therefore also used as a viability marker[14]. However, eight of these dyes were tested in a drug screen all showing IC50 values below 1μM with three, Mito Red, $DiOC_6$, and Rhodamine B being highly active against *P. falciparum* with IC50 values below 30 nM[15,16]. Additionally, in our hands MitoTracker signal can be diffuse, and therefore limit the resolution that is needed for the visualization of mitochondrial fission. Hence, we aimed to develop a reporter parasite line which harbors a fluorescent mitochondrial marker that

83 allows imaging of this organelle in live and fixed conditions in all life-cycle stages of *P.*
84 *falciparum*. To do this, we deployed a similar strategy that has been used successfully in the
85 rodent model *Plasmodium berghei*[17,18]. The targeting signal of the known mitochondrial
86 protein HSP70-3 was fused with a fluorescent protein and integrated in a silent intergenic
87 locus (SIL)[19]. Expression of this mitochondrial-localized fluorescent protein allowed
88 visualization of the organelle during imaging of asexual, sexual and mosquito stages. Using
89 high resolution confocal microscopy, we were able to make a detailed 3D map of different
90 mitochondrial fission stages during schizogony in asexual blood stages. Focused ion beam
91 scanning electron microscopy (FIB-SEM) image stacks from Evers *et al.* were used to confirm
92 these mitochondrial fission stages with high detail[20]. This also allowed us to study apicoplast
93 division and highlighted the potential role of the centriolar plaques (CPs) in apicoplast
94 segregation. These different microscopic approaches empowered us to put forward a
95 detailed model for mitochondrial and apicoplast division and distribution during the final
96 stages of schizogony.
97
98
99

Results

To acquire a detailed understanding of mitochondrial fission and distribution, we set out to capture this process throughout the *Plasmodium* life cycle by combining different microscopy approaches. We stained mature blood-stage wild-type *P. falciparum* NF54 strain parasites with two different MitoTracker dyes and used these to visualize the mitochondrion in fixed confocal imaging. Surprisingly, both MitoTracker dyes showed a discontinuous, punctate staining pattern (Figure 1A). FIB-SEM studies have confirmed the prevailing notion that the mitochondrion is a single, branched network during these schizont stages[20]. While this observation may arise from crosslinking of the MitoTracker dyes to specific proteins and aggregations thereof resulting from the fixation process, we concluded that the punctate staining pattern is likely an artifact and consequently limits our ability to dissect and visualize the process mitochondrial fission. To address this, we developed a new fluorescent mitochondrial marker that can be used for imaging live and fixed samples (Figure S1).

Design and generation of a new mitochondrial marker parasite line

We designed a mitochondrial marker that consists of the promotor and mitochondrial targeting sequence of the gene encoding the mitochondrial heat shock protein 70 (HSP70-3, PF3D7_1134000), fused to an mScarlet red fluorescent protein (Figure S1A). HSP70-3 was selected based on its high and consistent expression profile throughout the whole life cycle and has been successfully used for the same purpose in *P. berghei*[17,18]. We aimed to stably integrate this fluorescent marker in the *P. falciparum* genome, without affecting any normal biological processes and parasite growth throughout the parasite life cycle. Selection of the new integration site, SIL7, is described extensively in Supplemental Information S1. The integration plasmid was transfected into NF54 parasites together with two different Cas9 guide plasmids directed at the SIL7 site. Successful integration of the mitochondrial marker and absence of WT parasite contaminations were confirmed by integration PCR (Figure S1B). A growth assay showed no difference in growth of the mitochondrial reporter line, MitoRed, compared to WT parasites in asexual blood stages (Figure S1C).

Characterization of the MitoRed parasite line

To visualize the mitochondrial marker, asexual blood-stage MitoRed parasites were fixed and used for fluorescent imaging. The fluorescent signal was well preserved after fixation and no antibody staining was required for mitochondrial visualization in all asexual blood stages (Figure 1B). To assess whether the punctate mitochondrial morphology observed after MitoTracker staining was an imaging artifact or a morphological aberration caused by the dye, we stained MitoRed parasites with three different MitoTracker dyes. Discontinuous, punctate mitochondria were observed in all MitoRed parasites stained with MitoTracker, while this was not observed in unstained MitoRed parasites (Figure 1C). The effect was less pronounced during live imaging of MitoTracker stained parasites (Figure S2). While there is an obvious imaging artifact following fixation of MitoTracker-stained blood-stage *P. falciparum* parasites, the altered MitoRed signal in the presence of the dye might even suggest possible changes in mitochondrial morphology.

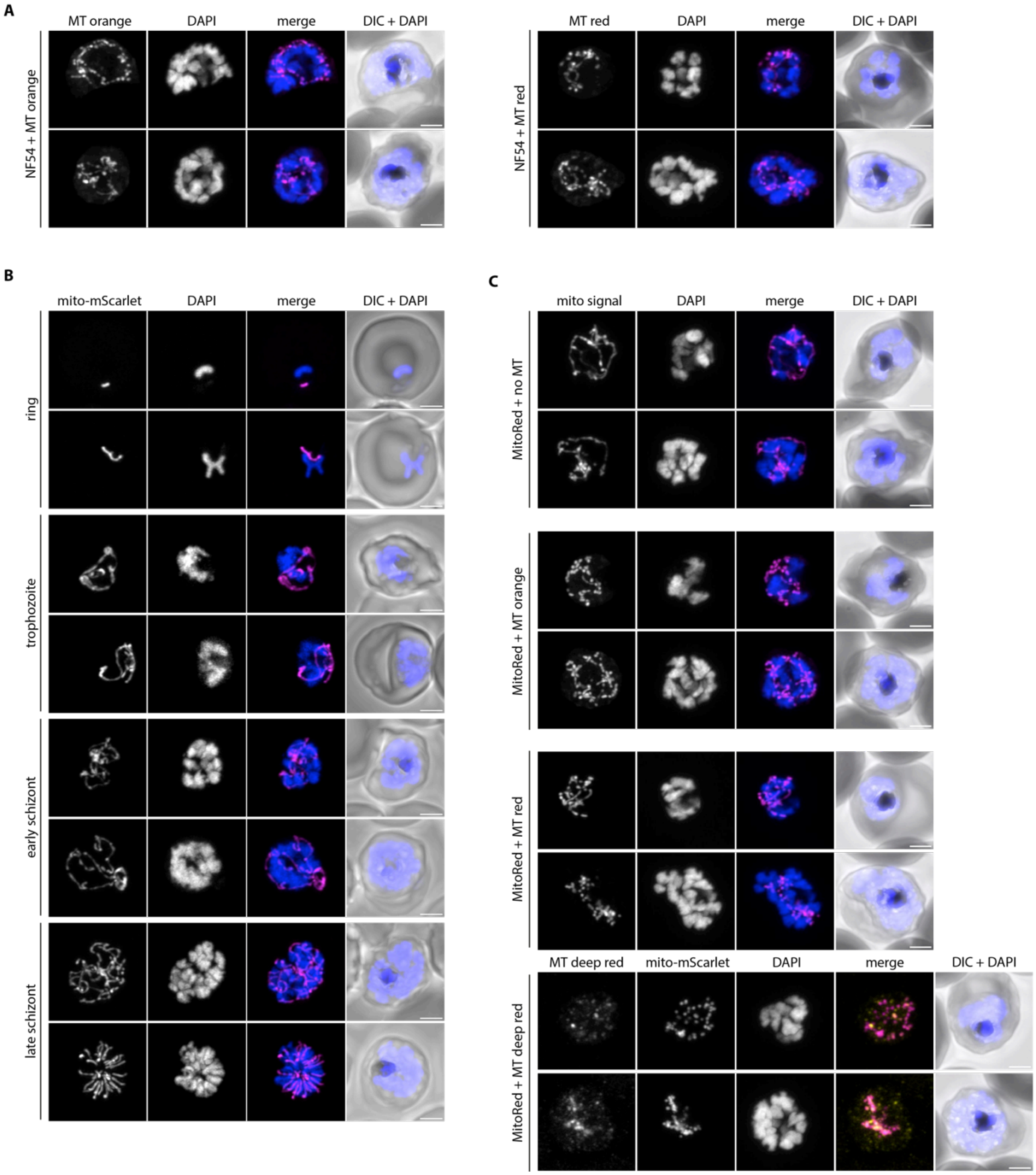

Figure 1. Comparison of MitoTracker and a new mitochondrial marker for fluorescence imaging. *A) Fluorescent imaging of WT parasites stained with MitoTracker Orange CMTMRos (MT orange) or MitoTracker Red CMXRos (MT red). B) Fluorescence microscopy of MitoRed. The mito-mScarlet signal was observed in all asexual life-cycle stages including rings, trophozoites, early and late schizonts. No antibody staining was used and fluorescent signal observed is exclusively the mito-mScarlet signal. C) Fluorescence microscopy of MitoRed, either unstained (no MT) or stained with MT orange, MT red or MitoTracker Deep Red FM (MT deep red). Mito signal is the combined MitoTracker and mito-mScarlet signal that is observed in this channel. DAPI (blue) is used to visualize DNA and DIC (differential interference contrast) for general cellular context. All images are maximum intensity projections of Z-stacks (41 slices, 150 nm interval) taken with Airyscan confocal microscope. Scale bars, 2 μm.*

157 **Mitochondrial dynamics during gametocyte development and activation**
158 To study mitochondrial dynamics throughout the malaria parasite life cycle, MitoRed
159 parasites were induced to form gametocytes, which were fixed for microscopy on day 5, 7,
160 10, and 13 post induction. Parasites were stained for α tubulin to distinguish male and
161 female gametocytes in stage IV and V. For each stage, between 11-19 parasites were
162 imaged over two independent experiments and described observations were consistent
163 over all analyzed parasites. In stage II and III gametocytes, the mitochondrion appears as a
164 small knot that increases slightly in size when gametocytes become more mature (Figure
165 2A). This is consistent with our FIB-SEM data[20]. Evers *et al*. also showed that gametocytes
166 have multiple mitochondria already from early gametocyte development onwards. Although
167 light microscopy does not provide the resolution or ability to show membrane boundaries to
168 distinguish the multiple mitochondria in stage II and III gametocytes, in stage IV
169 gametocytes we could clearly observe separate mitochondria in both male and female
170 gametocytes (Figure 2A, Figure S3A). There is no clear difference in stage IV gametocytes
171 between male and female mitochondria. However, in stage V gametocytes the mitochondria
172 in males appear slightly more dispersed, while the female mitochondria remain compact
173 (Figure 2A, Figure S3B). Data from Evers *et al.* support this and showed consistently smaller
174 volume and more loosely packed mitochondria in males compared to females[20]. When
175 gametocytes are taken up by the mosquito via a blood meal, they are activated and
176 transform into extracellular male and female gametes. While the female gametocyte
177 develops into a single macrogamete, male gametocytes form up to eight flagellated
178 microgametes. This transformation is triggered by a temperature drop, an increase in pH,
179 and xanthurenic acid present in the mosquito midgut[21]. Upon *in vitro* activation, the
180 difference between male and female mitochondria becomes more evident. Mitochondria in
181 females remain in a compact knot while the parasite rounds up (Figure 2B). Interestingly, in
182 males the mitochondria become smaller and more dispersed, and sometimes round up to
183 small bean-like structures (Figure 2B, Figure 2D). This process already starts 2 min after
184 activation. While this particular activation experiment was performed on a gametocyte
185 culture that did not exflagellate for unclear reasons, it was repeated twice, and very similar
186 results were found in exflagellating males (n=19) (Figure 2C). There was no significant
187 difference between number of exflagellation events in MitoRed parasites compared to NF54
188 parasites (Figure S4A). An association of mitochondria with flagella is not uncommon and
189 can also be observed in *e.g.* kinetoplastids, such as *Trypanosoma* and *Leishmania spp*, where
190 the mitochondrion resides at the base of the flagellum, and in human sperm cells, where
191 the mitochondrion wraps around the base of the flagellum to provide energy for flagellar
192 movement[22]. We found close apposition of the dispersed mitochondria to the axonemal
193 tubulin in all 19 exflagellating males that were analyzed (Figure S4B, S4C).
194
195 **Mitochondrial dynamics in mosquito stages**
196 In the mosquito midgut, the male microgamete seeks out a female gamete for fertilization.
197 After fertilization, the zygote takes one day to transform into a motile ookinete, which can
198 traverse the midgut epithelium and differentiate into an oocyst. This oocyst expands and
199 motile sporozoites are formed within the oocyst. When fully matured, the oocyst will burst
200 and sporozoites will egress, spread through the hemolymph system, and invade the
201 mosquito salivary glands. During oocyst development, the parasite mitochondrion has to
202 expand enormously and then be divided over thousands of daughter sporozoites. However,

203 very little is known about mitochondrial dynamics and only few studies have visualized the
204 mitochondrion during these stages[17,23,24].
205

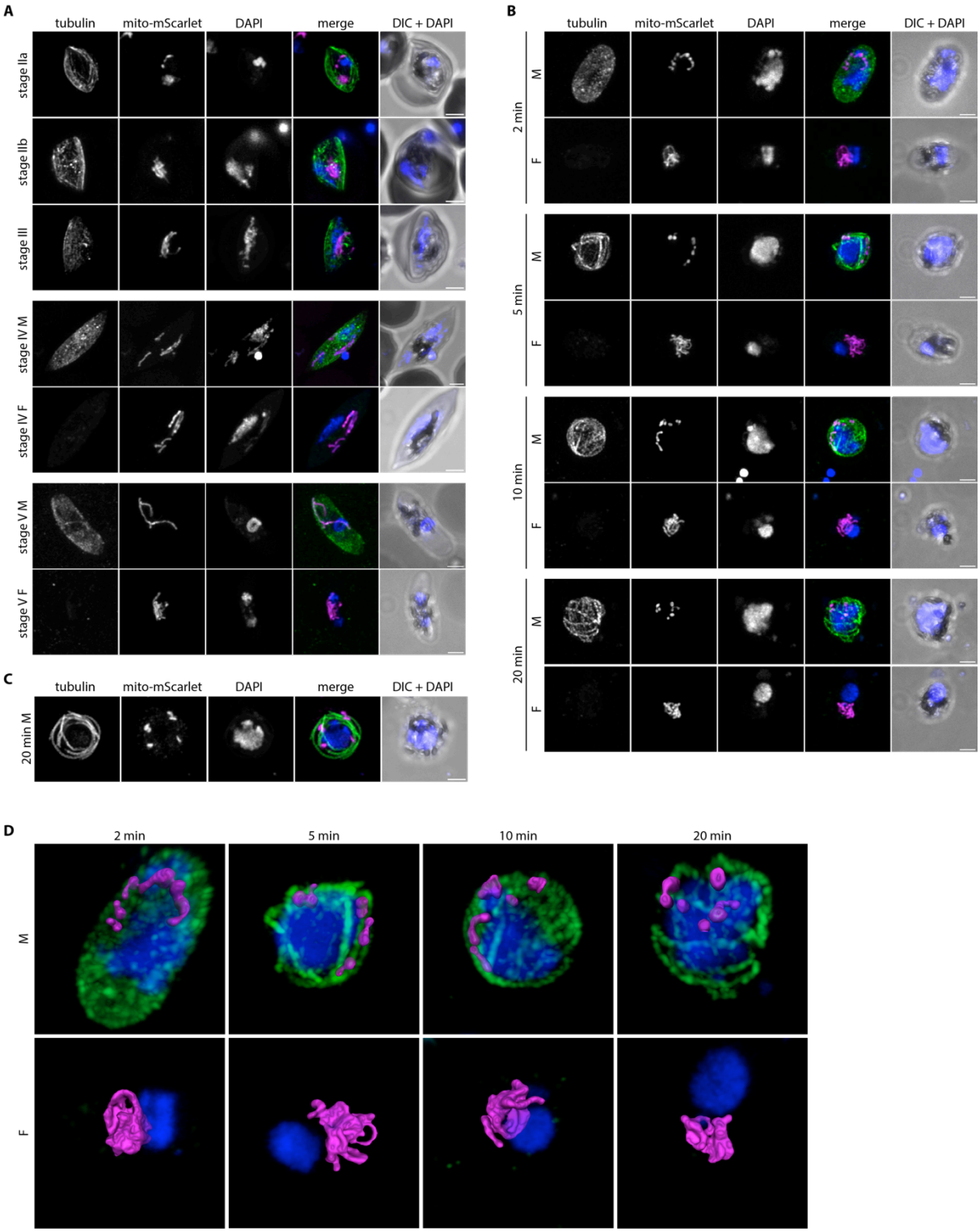

206
207
208 ***Figure 2. Mitochondrial dynamics during gametocyte development and activation.*** *A)*
209 *Immunofluorescence assay on MitoRed gametocytes stages IIa, IIb, III, IV, and V, stained with anti-β-*
210 *tubulin (green) and DAPI (DNA, blue). The mito-mScarlet signal is shown in magenta. In stage IV and V,*
211 *male (M) and female (F) gametocytes are distinguished based on the intensity of the tubulin signal (males*
212 *high, females low). B) Immunofluorescence assay on MitoRed parasites during different stages of*

gametocyte activation (2, 5, 10 and 20 min after activation). C) Immunofluorescence assay on MitoRed exflagellating male gamete 20 min after activation. A-C) Images are maximum intensity projections of Z-stacks (41 slices, 150 nm interval) taken with an Airyscan confocal microscope. Scale bars, 2 μm. D) 3D visualization of male and female MitoRed parasites 2, 5, 10, and 20 min after activation. The mito-mScarlet fluorescent signal is segmented based on manual thresholding.

To explore if MitoRed parasites develop normally in the mosquito and to visualize mitochondrial morphology, mature MitoRed gametocytes were fed to *Anopheles stephensi* mosquitoes. One day after the feed, the mosquito blood bolus was extracted and stained with anti-*Pf*s25 conjugated antibodies to visualize ookinetes by live microscopy. We distinguished different stages of ookinete maturation as described by Siciliano *et al.*[25]. Due to the resolution limit of light microscopy, it was difficult to tell if there were one or multiple mitochondria as observed in gametocyte stages. Since we did not find evidence for the presence of multiple mitochondria in these ookinete development stages, we will refer to it as "the mitochondrion" in the coming paragraph, although we cannot rule out the presence of multiple mitochondria. During earlier stages of ookinete development (II), when ookinetes have a short protuberance attached to the round body, the mitochondrion resides in the round body (Figure 3A, 3B). When the protuberance starts to elongate further, one elongated mitochondrial branch stretches out and reaches into the protuberance. In stage III ookinetes, the mitochondrion stretches out further into the growing protuberance, spiraling out from the round body. We could not find clear stage IV ookinetes where the protuberance is at its full length, which could be explained by the swift development from stage IV to V ookinetes as was observed by Siciliano *et al.*[25]. However, in the mature stage V ookinetes, the mitochondrion appears as a tight knot in the main parasite body.

At day 7, 10, and 13 after infection, mosquitoes from a feed with an infection rate of 100% and an average of 5 oocysts/mosquito were dissected and midguts were used for live confocal microscopy. At day 7, small oocysts (~10 μm diameter) were observed with a branched mitochondrial network stretched out throughout the cell (Figure S5A). Segmentation of the fluorescent signal based on manual thresholding indicated that the mitochondrion consisted of one continuous structure. Day 10 oocysts were much larger (~35 μm diameter) and the mitochondrial mesh-like network appeared more organized, also localizing to areas directly below the oocyst wall (Figure S5B). At day 13, oocysts of various sizes were observed. Some large oocysts (~70 μm diameter) showed a highly organized mitochondrial network, where mitochondrial branches were organized in a radial fashion around a central organizational point (Figure S5C). We named these points mitochondrial organization centers (MOCs). At least tens of these MOCs could be observed per cell. Some smaller oocysts (~35 μm diameter) at day 13 showed structures that looked like beginning MOCs (Figure S5D). However, several small oocysts showed a dispersed, globular mitochondrial signal, which we interpreted as unhealthy or dying parasite (Figure S5E). While several free sporozoites were observed in dissected midguts and salivary glands on day 16 (data not shown), we never observed an oocyst containing fully mature sporozoites with a divided mitochondrion or an infected salivary gland on day 16 and 21 after infection. This indicates that sporozoites are produced and released into the hemocoel, however, they have a health defect that prevents them from infecting the salivary glands. Possibly the mitochondrial marker or the integration in the SIL7 locus causes issues for sporozoite development. We conclude that the MitoRed line is a great tool for mitochondrial

visualization in asexual blood stages, gametocytes stages, and mosquito stages up until late oocysts (Supplemental Information S1) but that for studies later in the life cycle other tools need to be developed and tested.

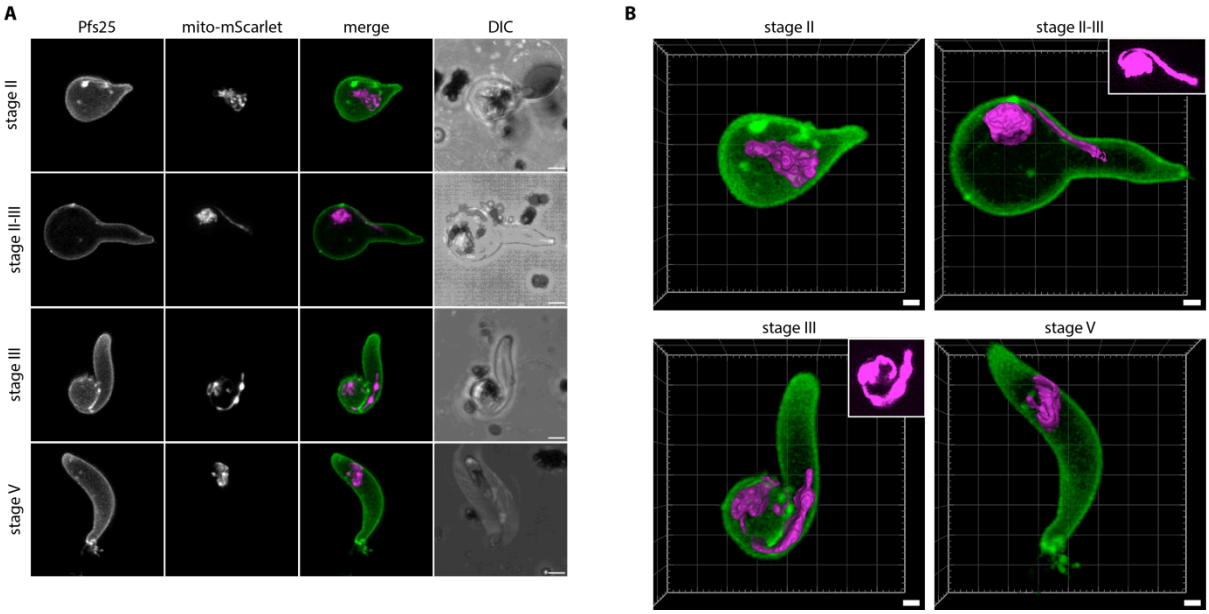

Figure 3. Mitochondrial dynamics during ookinete development. *A) Live imaging of MitoRed ookinetes one day after mosquito feed. Different stages of ookinete maturation (II – V) were distinguished based on description by Siciliano* et al.[25]*. Cells were stained with an Alexa fluor 488 conjugated anti-Pfs25 antibody to visualize parasite outline (green). Images are maximum intensity projections of Z-stacks (30 slices, 185 nm interval) taken with an Airyscan confocal microscope. Scale bars, 2 μm. B) 3D visualization of different ookinete maturation stages. The mito-mScarlet fluorescent signal is segmented based on manual thresholding. Two smaller images in upper right corner of stage II-III and stage III are crops of the mitochondrial fluorescent signal with increased brightness and contrast. Scale bars, 1 μm.*

Mitochondrial division during schizogony in asexual blood stages

Next, we aimed to use MitoRed for live visualization of mitochondrial division during schizogony in asexual blood stages. The biggest advantage of live imaging is that one parasite can be followed over time to capture mitochondrial fission events chronologically. Unfortunately, this proved to be challenging. All parasites imaged in several experiments for a duration exceeding 60 min exhibited significant morphological alterations, including mitochondrial swelling, fragmentation, and formation of vesicle-like structures, which indicate an unhealthy or dying parasite (Figure S6A). Additionally, we frequently observed parasites egressing from their red blood cells (RBCs) after approximately 45 min of imaging, indicating that imaged parasites are unhealthy (Figure S6B). Optimizing imaging conditions by reducing laser power, increasing time interval, better temperature control, and gassing of the imaging chamber with low oxygen mixed gas (3% O_2, 4% CO_2), did not improve parasite health during imaging. Therefore, we decided to go for a fixed imaging approach to capture mitochondrial division in asexual blood stages.

To capture mitochondrial fission, MitoRed parasites were tightly synchronized and fixed between 32-36 and 36-40 hours after invasion. In our culture system, MitoRed parasites have a replication cycle of approximately 40 hours, so we captured the last eight hours of schizont maturation before merozoite egress from the RBC. In order to distinguish the

295 precise stage of schizont maturation, we included an anti-GAP45 antibody staining.
296 Glideosome associated protein 45 (GAP45) is an inner membrane complex (IMC) protein
297 and is important for RBC invasion[26,27]. IMC formation starts at the apical end of a developing
298 merozoite during schizogony and continues to develop until it fully encapsulates the
299 daughter merozoite with its own IMC membrane[28,29]. We used the stage of IMC formation
300 and therefore merozoite segmentation as a marker for the maturity and age of the
301 schizonts. Based on IMC and DNA staining, we differentiated four stages of schizont
302 maturation: pre-segmentation (n=6), early-segmentation (n=9), mid-segmentation (n=15),
303 and late-segmentation (n=10, Figure 4).
304
305 We generated and classified Z-stack images of 40 schizonts, which allowed us to reconstruct
306 a timeline of mitochondrial fission. During pre- and early-segmentation stages, the branched
307 mitochondrial network stretches throughout the parasite. Only at the end of early-
308 segmentation stages, when the IMC is approximately halfway formed, the mitochondrion is
309 oriented around the food vacuole in the center of the parasite with its branches pointing
310 outwards in a radial fashion, creating a "cartwheel"-like structure (Figure 4). As the IMC
311 progresses further and schizonts enter the mid-segmentation stage, this mitochondrial
312 cartwheel structure is divided into smaller fragments, which maintain their radial branch
313 orientation into the segmenting merozoites. Only when IMC formation appears complete,
314 did we observe mitochondria that are entirely divided and distributed over the daughter
315 merozoites. This highlights the extremely late timing of this process. These mitochondrial
316 division stages were confirmed in a second, independent 3D imaging experiment (Figure S7).
317

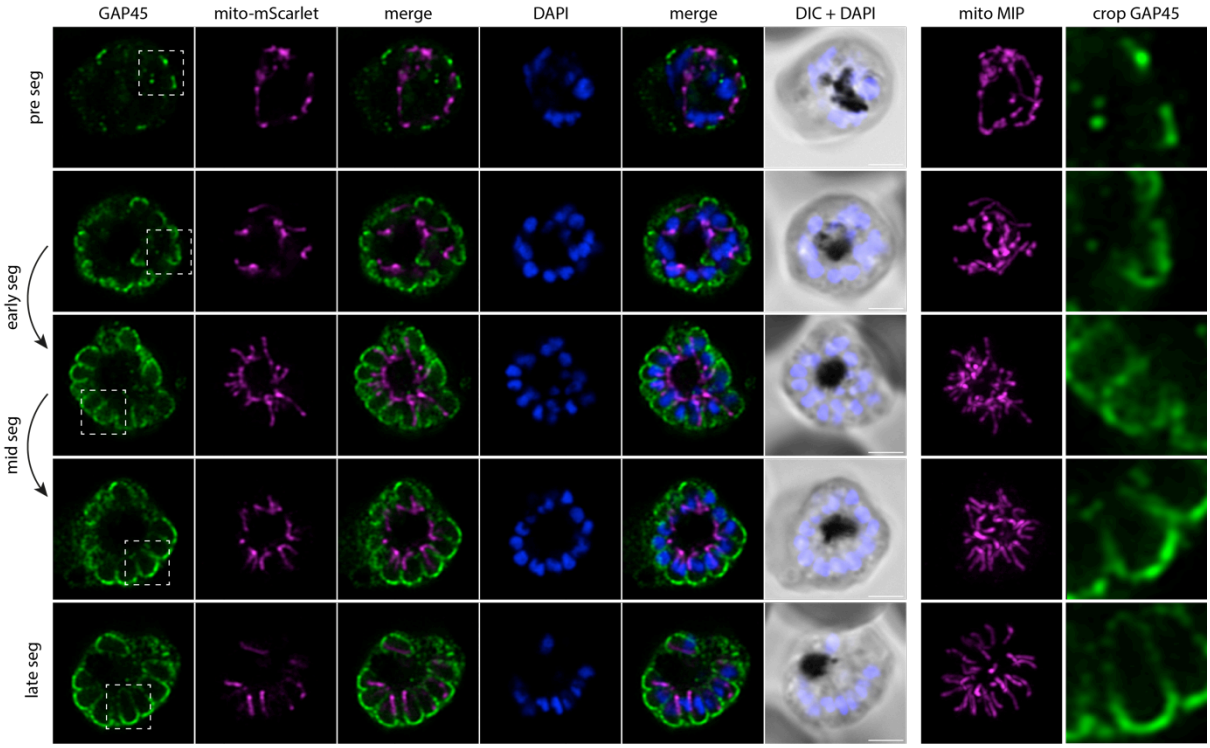

318
319
320 ***Figure 4. Mitochondrial fission in asexual blood-stage parasites.*** *Immunofluorescence assay on MitoRed*
321 *schizonts stained with anti-GAP45 antibody (green) to visualize IMC and DAPI (DNA, blue). The mito-*
322 *mScarlet signal is shown in magenta. Four different stages of schizont maturity are distinguished: pre-*
323 *segmentation (pre seg), schizonts still undergo nuclear division (nuclei are large and irregularly shaped)*
324 *and there is no, or very little IMC staining without clear curvature. Early-segmentation (early seg),*

schizonts have (almost completely) finished nuclear division (nuclei are small and round), there is a clear IMC signal that has a curved shape at the apical end of the forming merozoites but is less than half-way formed. Mid-segmentation (mid seg), the IMC of the segmenting merozoites in these schizonts is more than half-way formed, but there is still a clear opening at the basal end of the merozoite. Late-segmentation (late seg), in these schizonts the IMC seems to be completely formed with no clear opening at the basal end of the forming merozoites. Images are single slices of a Z-stack taken with an Airyscan confocal microscope. Images of the mito-mScarlet signal in the seventh column are maximum intensity projections (MIPs) (41 slices, 150 nm interval). Images in the eighth column are crops of the GAP45 signal depicted in the first column, indicated by the dotted-line areas. Scale bars, 2 μm.

To further quantify the numbers and sizes of mitochondria and to create 3D renderings of the mitochondrial network throughout segmentation, we utilized threshold-based masking of the fluorescent signal (Figure 5). During pre- and early-segmentation stages, the mitochondrial network consists of one large fragment (between 7-14 μm^3), often with 1-3 smaller fragments (<1.5 μm^3) (Figure 5AI, 5AII). As evident from our FIB-SEM data (Figure S10A), the mitochondrion features constricted regions, characterized by notably reduced diameters. Hence, the smaller fragments observed during these stages are likely not autonomous but caused by the reduced fluorescent marker intensity in the constricted regions. At the end of early-segmentation stages when the IMC is almost halfway formed, the mitochondrial network starts to orient itself in a radial fashion around the center of the parasite (Figure 5AII), consistent with the 2D image analysis (Figure 4). During mid-segmentation stages, the radial mitochondrial branches elongate further into the developing merozoites, and the large mitochondrial fragment is divided in smaller fragments at the center of the cartwheel structure (Figure 5AIII). There is a slight increase in number of mitochondrial fragments per parasite, specifically the "intermediate" sized mitochondrial fragments of 1-4 μm^3. Only in the last stage of merozoite segmentation, there is a big increase in the number of mitochondrial fragments (Figure 5C). Of note, there appears to be no correlation between this number and the number of nuclei in the parasites (Figure 5B, 5C). A likely technical explanation is the limited Z-resolution of light microscopy and the different nuclear and mitochondrial segmentation methods. When mitochondrial fragments are located closely above each other, the limited Z-resolution in combination with threshold-based masking can cause the adjacent fragments to appear as one continuous structure. Therefore, the number of mitochondrial fragments per schizonts will be underestimated in these late schizont stages. The nuclei on the other hand were segmented through an automated (spherical) object detection algorithm which does not have this problem. Even when the IMC formation appears to be completed based on the GAP45 staining, only 20% of cells appear to have concluded mitochondrial fission as indicated by exclusively containing homogenously small sized mitochondrial fragments (<1.0 μm^3) (Figure 5AIV). During the late segmentation stage, some parasites still have a large mitochondrial fragment of more than 5 μm^3, while others only have small and intermediate sized mitochondrial fragments (Figure 5D). This suggest that division of the mitochondrial cartwheel structure into small fragments is a fast, stepwise process that does not happen in a 2^n progression and happens only in the final moments of merozoite segmentation.

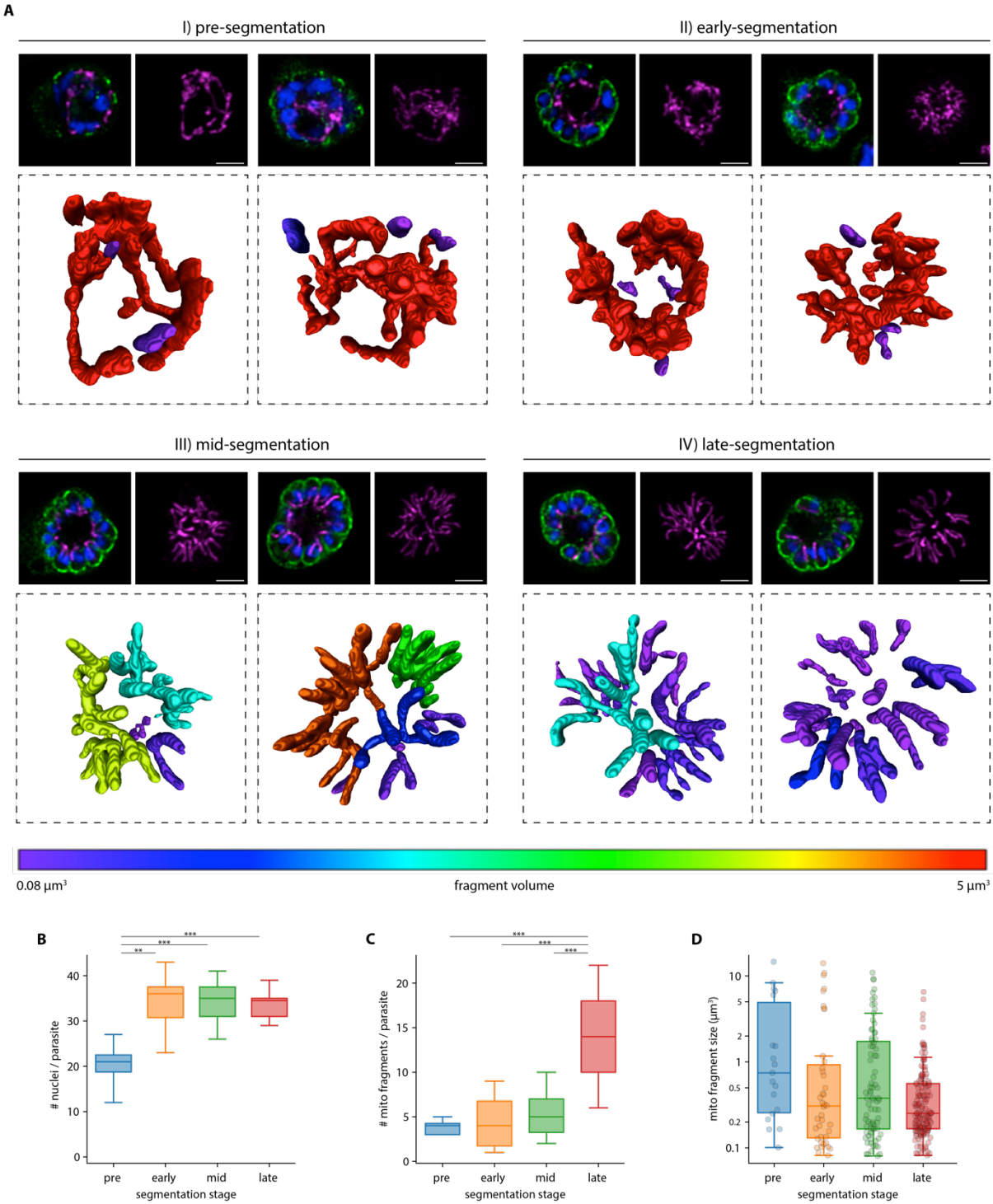

Figure 5. 3D analysis of mitochondrial fission stages during schizogony. *A) 3D visualization of mitochondrial segmentations based on thresholding of the mito-mScarlet signal in Arivis image analysis software. Smaller images in top row are a single slice of the Z-stack with anti-GAP45 labelling (IMC, green), DAPI (DNA, blue) and mito-mScarlet (magenta), and a maximum intensity projection of the mito-mScarlet signal. The larger bottom picture is a 3D visualization of the segmented mitochondrial signal. The color of the mitochondrial fragment represents the size of this fragment, as is shown in the color bar at the bottom. Two representative parasites are depicted for each of the four segmentation stages defined in Figure 4. Scale bars, 2 µm. B) Boxplot indicating the number of nuclei per parasite in the different segmentation stages. **, p<0.01; ***, p < 0.001. C) Boxplot indicating the number of*

*mitochondrial fragments per parasite in the different segmentation stages. ***, p < 0.001. D) Boxplot indicating the size of the mitochondrial fragments in the different segmentation stages.*

Visualization of mitochondrial and apicoplast division using volume electron microscopy

Although the use of light microscopy allowed us to reconstruct mitochondrial fission in good temporal resolution, its limited spatial resolution and reliance on indirect staining leaves some questions unanswered. Our recent volume electron microscopy study detailed parasite organelle structures at a nanometer resolution bringing many new insights to the light[20]. Here, we reused the underlying FIB-SEM data, which besides gametocytes also contains asexual blood-stage parasites from different stages, to examine mitochondrial fission with high resolution. Asexual parasites in different stages of schizogony were selected and organelles including nuclei, mitochondrion, and apicoplast were segmented for 3D rendering (detailed description per parasite in Tables S2 and S3). The mitochondrion and apicoplast can be recognized by their tubular shape in addition to the double membrane of the mitochondrion and the thicker appearance of the four membranes of the apicoplast. In line with the results from our light microscopy experiments, the mitochondrion is a large, branched network stretched throughout the cell in early schizont stages before segmentation has started (Figure 6, Movie 1). The apicoplast is also a branched network, however, it is much smaller than the mitochondrion (Table S2). The apicoplast network is divided into smaller fragments of different sizes when nuclear division is still ongoing and IMC formation has started (Figure 7, Table S3, Movie 4). When nuclear division is finishing and the IMC envelops part of the nucleus, apicoplast division is completed (Figure 6, Movie 5). The mitochondrion starts to orient its branches in a radial fashion towards the developing merozoites. When nuclear division is completely finished and the IMC envelops most of the nucleus, the mitochondrion forms a clear cartwheel structure with its branches pointing into the developing merozoites (Movie 6). During late segmentation stages, where only a small opening is connecting the merozoite to the residual body, the mitochondrion is divided into smaller fragments of various sizes (Movie 7). While some mitochondrial fragments have a volume comparable with the mitochondria in a fully segmented parasite (0.016 - 0.036 μm^3), other fragments are still 2-4 times that volume (FigureS8).* These larger mitochondrial fragments have several branches that are pointing into developing merozoites but are still connected to each other outside the merozoites. In an almost fully segmented schizont, where most merozoites are fully developed and only few merozoites are still connected to the residual body through a small opening, the mitochondrial division is completed and the number of mitochondrial fragments is the same as the number of merozoites (Movie 8). These findings corroborate our light microscopy data and confirm the mitochondrial division stages, position of relevant structures not stained in light microscopy, and timing of mitochondrial and apicoplast division during schizogony.

** Note: The volumes measured in the FIB-SEM data differ greatly from the volumes measured in the 3D fluorescent microscopy data. This can be explained by the limited spatial resolution of fluorescent microscopy because of the diffraction of light. The diffraction limit of the confocal Airyscan microscope that was used is ~120 nm in lateral direction and ~350 nm in axial direction. The diameter of the mitochondrion in asexual blood-stage parasites is ~140 nm, which is at the edge of the resolution limit. Therefore, the volume measurements of thresholding-based segmentation of the fluorescent signal are not very accurate and quickly over-estimate the volume. These volume estimations should merely be used to compare relative volumes of mitochondrial fragments. The FIB-SEM data has a resolution of 5 nm in lateral direction and 15 nm in axial direction, which allows much more precise visualization of organelles and volume measurements.*

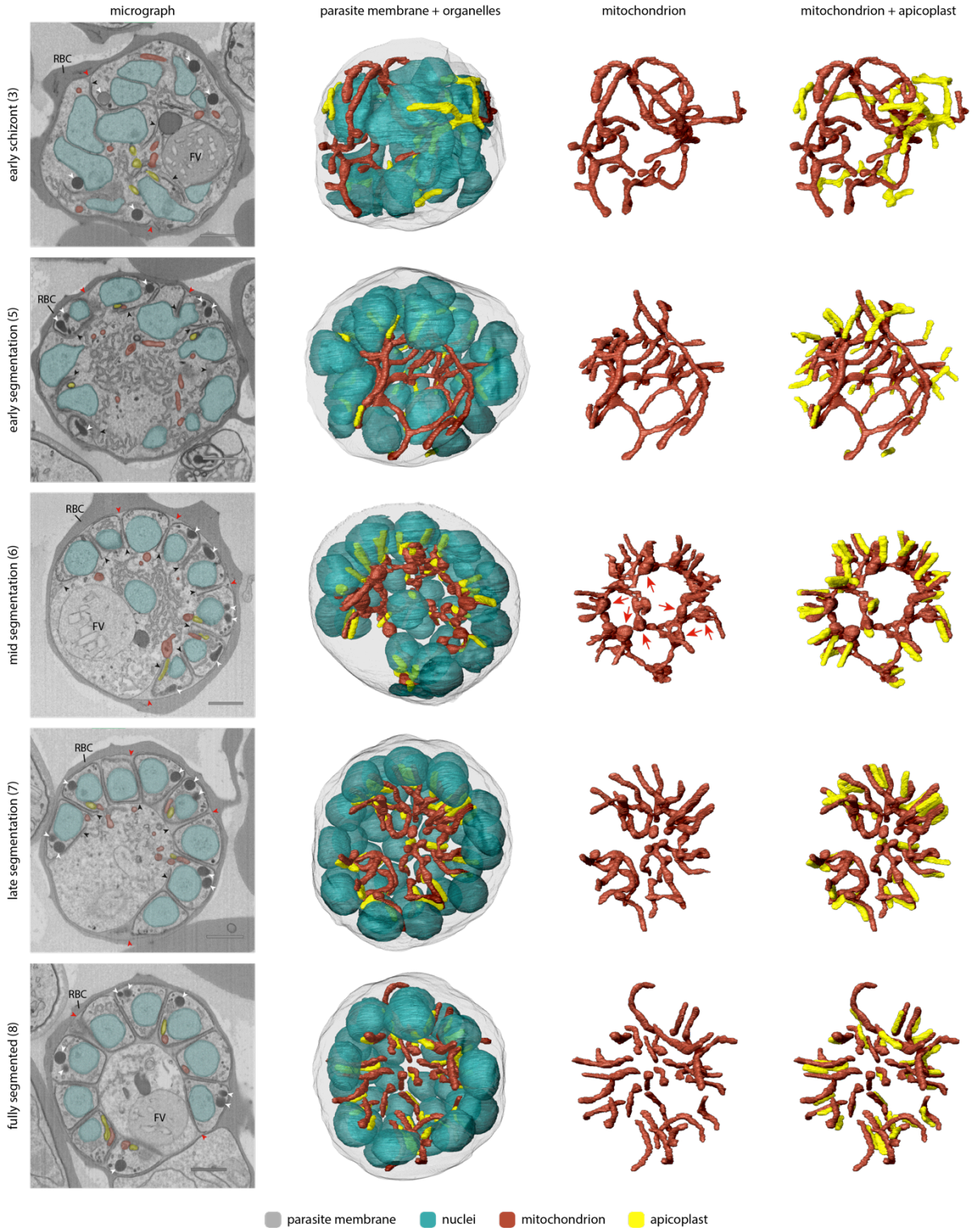

Figure 6. 3D rendering of mitochondrion and apicoplast during different stages of schizogony. *First column contains representative micrograph images from different schizont stages. The numbers between brackets indicate the parasite ID number and detailed information can be found in table S2 and S3. The red blood cell (RBC) and food vacuole (FV) are indicated by their abbreviations. Rhoptries are indicated by white arrowheads, parasitophorous vacuole membrane is indicated by red arrowheads, and parasite membrane invaginations are indicated by black arrowheads. Scale bars, 1 μm. The second, third, and fourth column contain 3D renderings of parasite membrane (gray, 5% transparency), nuclei (teal, 50% transparency), mitochondrion (red), and apicoplast (yellow). Red arrows indicate merozoite entrance bulins.*

440
441 **Interaction between mitochondrion and apicoplast in late stage schizonts**
442 During schizogony, the mitochondrion and apicoplast show different moments of close
443 association. Prior to apicoplast division, the mitochondrion and apicoplast have several
444 apposition sites, which have also been described by Evers *et al.*[20] (Figure S9A and S9B). It
445 remains unclear if these close associations represent true membrane contact sites that
446 facilitate the exchange of metabolites or lipids between the organelles, or if these are
447 merely random due to the limited space in the parasite. When apicoplast division is finished,
448 the endings of the mitochondrial branches reach towards the basal endings of the
449 apicoplasts (Figure S9D). Subsequently, the branches of the mitochondrial cartwheel
450 structure align with the apicoplast over its entire length (Figure S9C and S9D). This close
451 alignment remains when mitochondrial division is complete.
452
453 **Bulbous mitochondrial structures with double membrane invaginations**
454 The parasite mitochondrion does not have a consistent diameter during schizogony. While
455 some parts have a very small diameter other areas of the mitochondrion are more bulbous
456 (Figure S10A). These bulbous parts often contain double membrane invaginations of various
457 size and shape (Figure S10C, S10D, S10F). These bulbous invagination structures (bulins) are
458 found in all schizont stages and vary greatly in shape, size, and location in the mitochondrial
459 network. In early stage schizonts, bulins can be found at branching points and in the middle
460 of a continues branch of the mitochondrial network (Figure S10D, S10F). However, during
461 mid-segmentation stages, when the mitochondrion is oriented in its typical cartwheel
462 structure, bulins are consistently observed at the base of a mitochondrial branch near the
463 merozoite entrance (Figure 6, Figure S10D, S10F). These merozoite-entrance bulins were
464 found in all eight mid-segmentation stage schizonts from two independent experiments
465 (example shown in Movie 9). Bulbous areas at the base of mitochondrial branches are also
466 observed with fluorescent microscopy (Figure S10B). This, and the specific location of bulins,
467 makes them unlikely an artifact of fixation or sample preparation for the FIB-SEM, although
468 this cannot be ruled out completely. Bulins that reside at the entrance of a forming
469 merozoite during the cartwheel phase are typically characterized by contact with the basal
470 end of the divided apicoplast, and a small constriction right above the bulin where the
471 mitochondrial branch enters the merozoite (Movie 10). Bulbous areas at the base of the
472 mitochondrial branches are also observed with fluorescent microscopy (Figure S10B). In
473 late-segmentation schizonts, we observed small bulins at the base of a divided
474 mitochondrial fragment or at the entrance of a merozoite when the mitochondrial branch
475 was not yet divided (Figure S10D, S10F). Sporadically, we also found bulins in the apicoplast
476 (Figure S10E). The significance and function of these bulins remain to be explored, but it is
477 tempting to speculate about a possible role in organelle division.
478
479 **Centriolar plaques associate with apicoplast but not mitochondrion during organelle**
480 **segregation**
481 In mammalian cells, segregation of organelles is coordinated by microtubules that arise
482 from the centrosomes, or so-called microtubule organizational centers (MTOCs).
483 *Plasmodium* parasites lack canonical centrosomes but organize their mitotic spindle from a
484 structure called the centriolar plaque (CP), which is embedded in the nuclear envelope[30,31].
485 Expansion microscopy studies from Liffner *et al.* have suggested an association of the CPs
486 with both the mitochondrion and the apicoplast during schizogony, suggesting their

involvement in organelle segregation[32]. In our FIB-SEM images, we can distinguish the CP by electron dense coffee filter-shaped regions in the nucleus (Figure 7A). In an early schizont that still lacks IMC or rhoptries, nuclei contain one or two CPs, which are oriented to the periphery of the parasite. 3D renderings show no direct association between the CPs and the mitochondrion or apicoplast (Figure 7B, Movie 1). Although the distances between the mitochondrion and CPs (average 616 nm, SD 235 nm) in this early schizont are significantly smaller than the apicoplast-CPs distances (average 1350 nm, SD 260 nm), there is no direct interaction between the mitochondrion and CPs since the smallest CP-mitochondrion distance measured is 332 nm. The significant difference can be explained by the fact that the apicoplast is located in the center of the parasite, while the mitochondrion is larger and stretched throughout the whole cell leading to coincidental closer proximity to the peripheral CPs. In slightly later stage schizonts where IMC and rhoptry formation has started, all nuclei contain either two CPs, or one CP that is dividing. A portion of the CPs associated with the apicoplast, specifically with the endings of apicoplast branches (Movie 2). When the IMC is developed slightly further, all CPs associate with the apicoplast over the total length of the peripherally localized apicoplast network (Movie 3). While two CPs from the same nucleus usually associate with one apicoplast branch (Figure S11A), sometimes these associate with completely different branches of the apicoplast network (Figure S11B). Furthermore, the distances between the CPs and apicoplast are significantly smaller (42 nm average, SD 46 nm) compared to those measured in earlier stages as well as to the unchanged CP-mitochondrion distances (663 nm average, SD 274 nm) (Figure 7B). The association between CPs and apicoplast continues during and after apicoplast division (Movie 4-7). After apicoplast division, each apicoplast fragment is associated with one CP at its peripheral end (53 nm average distance, SD 37 nm) (Movie 5). During mid-segmentation stages, the endings of the mitochondrial branches are close to the CPs (202 nm average distance, SD 65 nm) (Movie 6). However, this seems to be a result of the close association of the mitochondrion with the apicoplast, rather than a direct interaction between the mitochondrion and the CPs. In a fully segmented schizont, the CPs were much smaller and did not show a clear extranuclear compartment (Movie 8). This close and very consistent association between the apicoplast and the CP, suggest an important role in apicoplast segregation, while the mitochondrion likely deploys different mechanisms to accomplish its proper distribution over the forming merozoites.

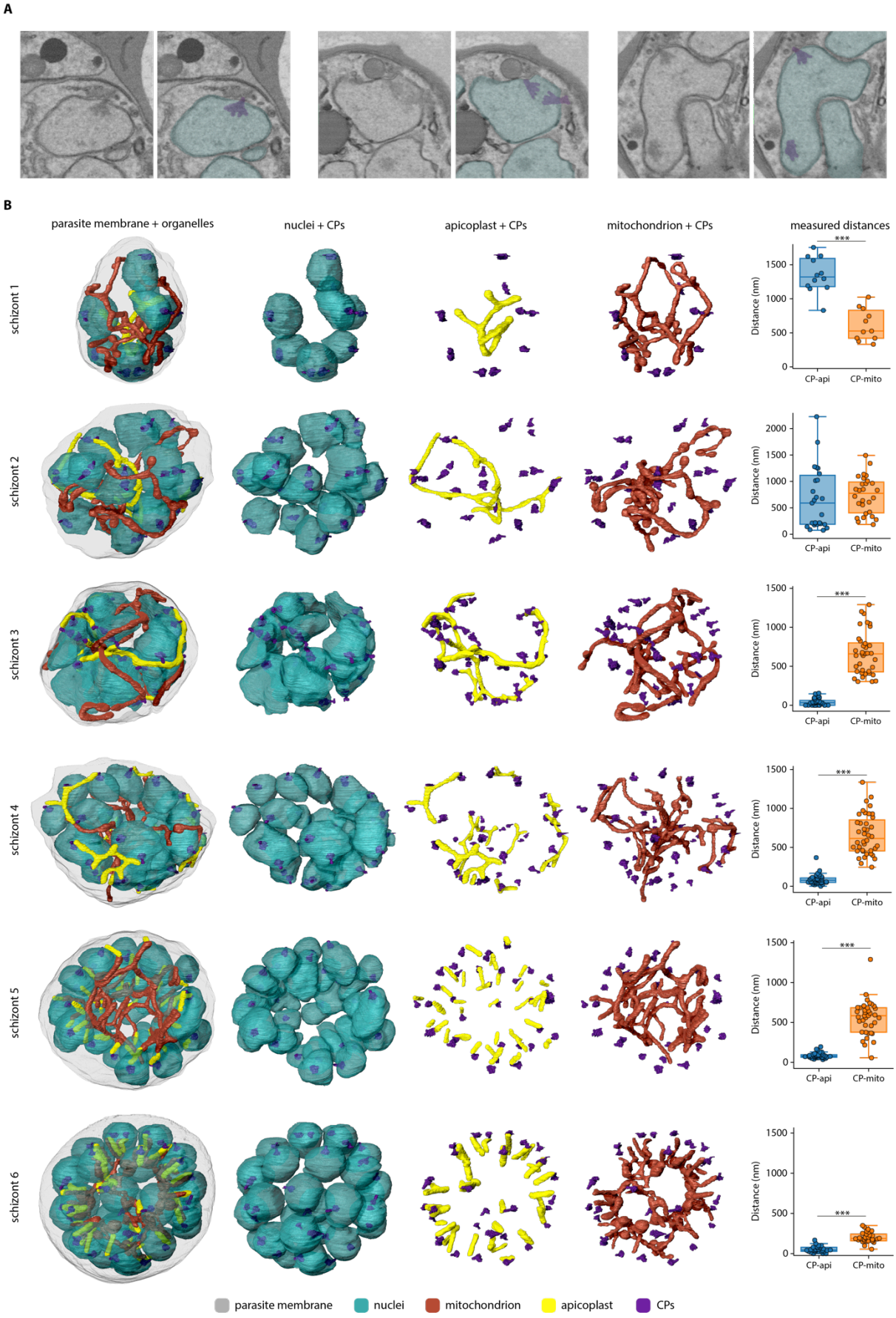
A
B
parasite membrane + organelles
nuclei + CPs
apicoplast + CPs
mitochondrion + CPs
measured distances
schizont 1
schizont 2
schizont 3
schizont 4
schizont 5
schizont 6
Distance (nm)
CP-api
CP-mito
***
parasite membrane
nuclei
mitochondrion
apicoplast
CPs

522
523

524 ***Figure 7. Association of apicoplast and not the mitochondrion with centriolar plaques during schizont***
525 ***development.*** *A) Micrographs of nuclei (teal) with centriolar plaques (CPs, purple). B) 3D rendering of*
526 *nuclei (teal), apicoplast (yellow), mitochondrion (red), CPs (purple), and parasite membrane (gray, 5%*
527 *opacity). Parasite ID numbers are indicated on the left side of the micrograph images. Right column shows*
528 *measured distances between CPs and closest point to the apicoplast or mitochondrion. ***, $p < 0.001$.*
529
530
531
532

533 ## Discussion

534 In contrast to most eukaryotes, the fast-replicating *P. falciparum* asexual blood-stage
535 parasites harbor only a single mitochondrion. Consequently, proper division and distribution
536 of this organelle during schizogony is crucial to ensure all daughter cells receive a
537 mitochondrion. Here, we visualized the poorly understood mitochondrial dynamics in blood
538 and mosquito stages using a new parasite line with a fluorescent mitochondrial marker and
539 super-resolution 3D imaging methods. During blood-stage schizogony, a cartwheel structure
540 is formed and divided into smaller, unequally sized mitochondrial fragments in a stepwise
541 process. Final division into single mitochondria happens during the last stage of merozoite
542 segmentation. These division steps were cross validated by analyzing available FIB-SEM data
543 with nanometer resolution. This also allowed us to reconstruct apicoplast division and its
544 interactions with the mitochondrion. Finally, we showed that the apicoplast but not the
545 mitochondrion associates with the CPs during merozoite formation.
546
547 To date, the visualization of *Plasmodium* mitochondria has largely relied on MitoTracker
548 dyes. However, these dyes are toxic at nanomolar concentrations[15,16] and our data suggest
549 that they may alter mitochondrial morphology (Figure 1). We developed a reporter parasite
550 line harboring a fluorescent mitochondrial marker that shows a more continuous and less
551 punctate staining pattern compared to MitoTracker dyes and is compatible with live and
552 fixed imaging without necessitating antibody labeling. Unfortunately, MitoRed is not well
553 suited for long-term time lapse imaging (>1h) since parasites showed various signs of poor
554 health, probably due to phototoxicity. While expansion microscopy is currently not feasible
555 with MitoRed, addition of a linear epitope tag would make this marker compatible with the
556 required denaturation step.
557
558 In line with our earlier observations, we demonstrated multiple mitochondria in gametocyte
559 stages[20]. As discussed by Evers *et al.*, there are several possible reasons for the emergence
560 of multiple mitochondria in gametocytes, such as adaptation to a metabolically varied
561 environment, distribution mechanism of mtDNA, or management of reactive oxygen
562 species. We expand upon these observations by also imaging gametocytes during activation.
563 In males, mitochondria become more dispersed while female mitochondria remain in a tight
564 knot. One possible explanation for this is that mitochondria in males are distributed to
565 specific locations in the cell to provide energy locally for certain processes. In sperm cells,
566 the mitochondrion resides at the base of the flagellum to provide energy for flagellar
567 movement[22]. While we observed close apposition of the mitochondria with axonemal
568 tubulin in some activated males using light microscopy (Fig. S4), this was not consistently
569 observed in all males, and we lack the resolution to prove real association. Another
570 explanation could be that the parasite undergoes a form of mitophagy as a source for
571 proteins, lipids, and nucleotides required for the rapid nuclear division and microgamete
572 formation. Even though mitophagy has not been studied in *Plasmodium*, some homologues
573 of the general autophagy pathway have been identified[33]. Autophagy as a survival
574 mechanism was described for *P. falciparum* and *T. gondii* under starvation conditions[34,35]. In
575 *T. gondii*, the fragmentation of the mitochondrion was reversed by using the established
576 autophagy inhibitor 3-methyl adenine[34]. Alternatively, the distribution of the mitochondria
577 could merely be a consequence of the nuclear expansion in the cell.
578

579 Mitochondrial dynamics during mosquito stages is poorly understood and to our knowledge
580 studies have thus far been restricted to *P. berghei*[17,23,24,36]. Here, we visualized the
581 mitochondrion in *P. falciparum* during mosquito stages for the first time. In early oocyst
582 stages, the mitochondrion resembles the extensively branched network from asexual blood-
583 stage schizonts. During oocyst development, the mitochondrial network organizes into
584 multiple MOCs that resemble the cartwheel structure observed in asexual blood stages.
585 Although these mitochondrial observations should be interpreted with care since oocysts
586 did not form salivary gland populating sporozoites and might therefore not be representing
587 healthy oocysts (see the supplement for a more extensive discussion), in *P. berghei* liver-
588 stage schizonts, a very similar mitochondrial organization was observed in sub-
589 compartments created by large membrane invaginations[12,37]. Similar sub-compartments are
590 present during oocyst development[37]. Based on apicoplast visualizations in *P. berghei* and
591 our observations of the formation of MOCs during oocyst stages, mitochondrial and
592 apicoplast dynamics in these sub-compartments in both oocyst and liver stages resemble
593 the dynamics of these organelles in blood-stage schizogony[12,38,39].
594
595 Although the use of new imaging techniques, such as expansion microscopy and 3D volume
596 EM, have revealed new insights in mitochondrial dynamics, many questions about the
597 timing and organization of mitochondrial division remained unanswered[11,32]. In an earlier
598 literature review, we proposed three possible mitochondrial division models: synchronous
599 fission, outside-in fission, or branching point fission[9]. Here, we used a new mitochondrial
600 marker and advanced imaging techniques, such as Airyscan confocal microscopy, to
601 reconstruct mitochondrial fission during schizogony. The use of volume EM provided the
602 resolution required to verify our fluorescence-based mitochondrial fission model while
603 simultaneously shedding light on the division of the second endosymbiotic organelle, the
604 apicoplast. This allows us to propose a new, detailed model of the organellar division and
605 segregation (Figure 8).
606
607 In this model, we describe the cartwheel orientation of the mitochondrion, its non-
608 geometric 2^n division, the late timing of division, and its association with the apicoplast. The
609 apicoplast divides when nuclear division is still ongoing and merozoite segmentation has just
610 started. Similar to the mitochondrion, its division does not happen in a geometric 2^n
611 progression, but different sized apicoplast fragments are observed in a mid-division stage.
612 The timing and orientation of the apicoplast-mitochondrion appositions, suggest a potential
613 role of the apicoplast in mitochondrial segregation. However, doxycycline treated parasites,
614 that have lost their apicoplast and are chemically rescued by isopentenyl pyrophosphate
615 supplementation, can still produce viable merozoites, suggesting that association with the
616 apicoplast is not essential for mitochondrial segregation[40]. The specific types of membrane
617 contact between both endosymbiotic organelles, whether these consist of direct physical
618 contacts, membrane fusions or tethering proteins, may vary and remain to be explored.
619 However, EM tomography data from Sun *et al*. show there are hints of connecting
620 structures between the mitochondrion and apicoplast in areas where the distance between
621 the organelles is very small and similar to the distance between the inner and outer
622 membranes of the organelles themselves in merozoites, suggesting physical link between
623 the organelles.
624

625 In other eukaryotic models, mitochondrial fission is facilitated by adaptor proteins on the
626 cytoplasmic side of the outer mitochondrial membrane that recruit dynamin GTPases, which
627 in turn oligomerize to form a constrictive ring around the organelle[9]. The only conserved
628 adaptor protein in *P. falciparum*, Fission 1 (Fis1), is dispensable in asexual blood stages
629 precluding an essential role in mitochondrial fission during schizogony[41]. Malaria parasites
630 also harbor three dynamin-related proteins[9]. As the timing of the apicoplast division
631 precedes that of the mitochondrion, it is conceivable that (parts of) the same dynamin-
632 based machinery may be reused for mitochondrial fission. Indeed, in a recent pre-print *P.*
633 *falciparum*, dynamin 2 (*Pf*DYN2) was shown to mediate both apicoplast and mitochondrial
634 fission[42]. Which other proteins comprise the mitochondrial division machinery in *P.*
635 *falciparum* remains to be explored.
636
637 Their morphological features, timing of appearance, and specific location at the entrance of
638 the developing merozoite during mid-segmentation stages suggests that the bulbous
639 invagination structures, or bulins, could play a role in mitochondrial fission. A role in the
640 distribution of certain components – e.g. mitochondrial DNA, proteins, or protein complexes
641 – to the branches of the mitochondrial cartwheel structure that enter the merozoite is also
642 conceivable. However, in earlier stages, bulins are also found at branching points or in
643 continuous parts of the mitochondrion and apicoplast, perhaps suggesting possible roles in
644 more general membrane remodeling of the organellar network.
645
646 We also observed CPs, the *P. falciparum* analogue of the centrosome, which function as
647 microtubule organizing centers and are important for mitosis and cell cycle regulation[43,44]. In
648 *T. gondii*, the centrosome associates with the apicoplast and ensures correct segregation of
649 the organelle during daughter cell formation[45,46]. Recent expansion microscopy data
650 suggested interaction of the CP with both the apicoplast and the mitochondrion in *P.*
651 *falciparum*[32]. From the onset of IMC and rhoptry formation, we observed close apposition of
652 the CPs and apicoplast, but not the mitochondrion (Figure 8). This CP-apicoplast association
653 continues during and after apicoplast division, indicating a role of the CPs in apicoplast
654 segregation. In other apicomplexan parasites, such as *Toxoplasma gondii* and *Sarcocystis*
655 *neurona*, centrosomes have also been indicated to be involved in apicoplast organization
656 and distribution during cell division[45,47]. The initial absence of CP-apicoplast association and
657 the later association of two CPs from one nucleus with separate apicoplast branches
658 suggests an active recruitment strategy. Motor proteins facilitate intracellular transport of
659 organelles along the cytoskeleton in multicellular eukaryotes. While dynein and kinesin
660 facilitate organelle transport along microtubules, myosin motor proteins transport
661 organelles along actin filaments to specific locations in the cell[48]. Previous studies have
662 shown a critical role of F-actin and myosin F in the inheritance of the apicoplast in *P.*
663 *falciparum* and *T. gondii*[49–52]. In *T. gondii* parasites that lack myosin F, the apicoplast fails to
664 associate with centrosomes[53]. Therefore, we hypothesize that myosin facilitates recruitment
665 of the apicoplast branches over the actin filaments to the CPs. Although the mitochondrion
666 is close to the CPs in late segmentation stages, the distance is always significantly bigger
667 than the apicoplast-CP distance. Additionally, mitochondrial branches reach much further
668 into the merozoites when fully segmented, compared to the apicoplast. Furthermore,
669 conditional knockout of *PfACT1* (actin-1) did not alter mitochondrial morphology in asexual
670 blood-stage schizogony[49]. Therefore, it remains questionable if the mitochondrial branches
671 are recruited to the CP via a similar mechanism as the apicoplast.

Volume EM is a powerful tool to study biological questions as it allows the visualization of complex, connecting structures and gives spatial and cellular context. Here, we reused available FIB-SEM data, which contains sexual and asexual blood-stage malaria parasites from many different stages of intra-erythrocytic development. Future reinterrogation of the data could facilitate in answering other biological questions that are beyond the scope of this paper, such as rhoptry biogenesis and development of the apical complex.

In this study, we have developed a reporter parasite line harboring a fluorescent mitochondrial marker – integrated in a new genomic locus – that can be used for mitochondrial visualization in blood and early mosquito stages. This allowed us to visualize mitochondrial division in unprecedented detail and describe the relative timing and of mitochondrial fission and segregation using high-resolution confocal microscopy and FIB-SEM image analysis. Combined with new insights in apicoplast division, mitochondrial and apicoplast interactions, and association of the apicoplast with the CP during schizogony, this allowed us to propose a new, detailed model of apicoplast and mitochondrial division during schizogony. These findings pave the way to home in on the molecular mechanisms underpinning mitochondrial and apicoplast division and segregation.

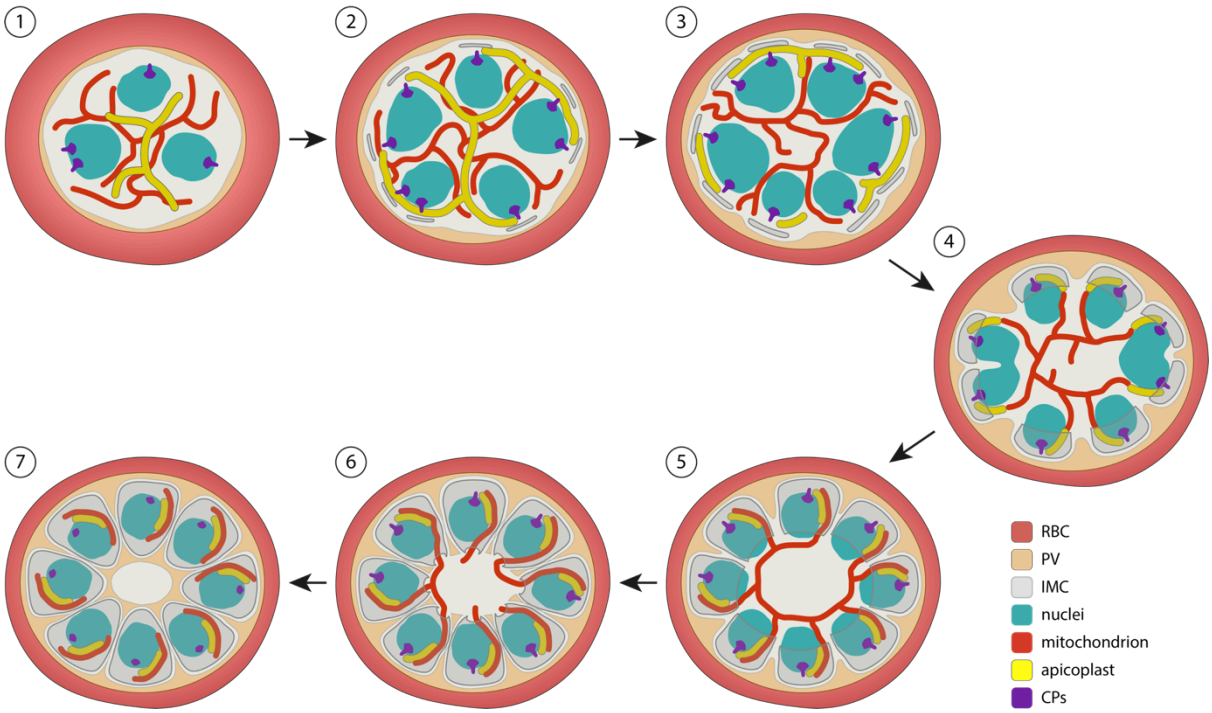

Figure 8. Schematic model for mitochondrial and apicoplast division and segregation in* P. falciparum *during schizogony. *(1) Nuclear division is ongoing, while inner membrane complex (IMC) formation has not started and both the mitochondrion and apicoplast are branched networks. The apicoplast localizes more to the center of the cell, while the mitochondrion is stretched throughout the whole cell. (2) When IMC formation starts, the apicoplast branches associate with the centriolar plaques (CPs) at the periphery of the parasite. (3) The apicoplast divides in a non 2^n progression, while it keeps its interaction with the CPs. (4) When nuclear division is finishing, apicoplast division is completely finished. The apical end of the apicoplast fragments associate with the CPs, while mitochondrial branches associate with the basal end of the apicoplast fragments. (5) The IMC develops further and envelops large parts of the nuclei. The mitochondrion orients itself in a cartwheel structure, while its branches align with the apicoplast fragments. (6) IMC formation is almost finished, and just a small opening connects the merozoites to the residual body. The mitochondrion divides in a non 2^n progression. The apicoplast still associates with the CPs and aligns with mitochondrial branches/fragments. (7) Merozoite segmentation is complete, the apicoplast loses its clear association with the CPs since they become smaller and do not have a clear extra nuclear compartment anymore. The mitochondrion is fully divided and still aligns with the apicoplast. Red blood cell (RBC), parasitophorous vacuole (PV).*

710 # Materials and Methods

711 **_P. falciparum_ culture and transfections**

712 *P. falciparum* NF54 and MitoRed parasites were cultured in RPMI1640 medium
713 supplemented with 25 mM HEPES, 10% human type A serum and 25 mM $NaHCO_3$ (complete
714 medium). Parasites were cultured in 5% human RBCs type O (Sanquin, the Netherlands) at
715 37°C with 3% O_2 and 4% CO_2. For transfection, 60 µg of homology-directed repair plasmid
716 was linearized by overnight digestion, precipitated, and transfected with 60 µg Cas9 plasmid
717 using ring transfection[54,55]. Briefly, a ring-stage sorbitol synchronized parasite culture was
718 transfected with the plasmids by electroporation (310 V, 950 µF). Five hours after
719 transfection, parasites were treated with 2.5 nM WR99210 for five days. Success of
720 transfection was assessed by integration PCR (Fig S1, Table S1).
721

722 **Plasmid constructs**

723 To generate the base SIL7 reporter plasmid (pRF0057) the 5' and 3' homology regions for
724 SIL7 were amplified from genomic NF54 DNA (Table S1) and cloned into the pBAT
725 backbone[19] with NgoMIV and AleI (5') and BmgBI and AatII (3'). For the final MitoRed repair
726 plasmid, first the mScarlet sequence was amplified from p1.2RhopH3-HA-mScarlet (a kind
727 gift from Prof. Alan Cowman)[56] (Table S1). The mScarlet sequence was cloned into pRF0077
728 (empty tagging plasmid with PBANKA_142660 bidirectional 3'UTR) with AflII and EcoRI
729 restriction sites, generating pRF0078 intermediate plasmid. The HSP70-3 promotor (prom)
730 and targeting sequence (t.s.) sequence was cloned into pRF0078 with EcoRI and NheI
731 restriction sites, generating pRF0079 intermediate plasmid. The whole mitochondrial
732 marker (HSP70-3 prom + t.s. + mScarlet) was cloned from pRF0079 into pRF0057 with EcoRI
733 and AflII restriction sites, generating pRF0191, the final repair plasmid. CRISPR-Cas9 guide
734 plasmids targeting two different sites in the SIL7 region were generated. Guide
735 oligonucleotides were annealed and cloned into pMLB626 plasmid (a kind gift from Marcus
736 Lee)[57] using BbsI restriction enzyme, generating the two final guide plasmids (Table S1).
737

738 **Growth assay**

739 NF54 WT and MitoRed parasites were synchronized using 63% Percoll centrifugation. Late-
740 stage parasites were isolated from the Percoll gradient and added to fresh RBCs. Four hours
741 later, a 5% sorbitol synchronization was performed, which allowed only young rings that just
742 invaded a new RBC to survive. Ring-stage parasites were counted and three independent
743 cultures of 0.05% parasitemia were set up for each parasite line. Every 24 hours, 10 µl
744 culture was taken and fixed in 100 µl 0.25% glutaraldehyde in PBS up until day 5. To prevent
745 overgrowth, parasite cultures were cut back 1/50 after samples were taken on day 3. Before
746 readout, fixative was taken of, and parasite DNA was stained with 1:10,000 SYBR Green in
747 PBS. Parasitemia was determined by measuring SYBR Green positive cells with a Cytoflex
748 flow cytometer (Beckman Coulter Cytoflex) using the 488 nm laser. Final parasitemia on day
749 4 and 5 was adjusted for the 1/50 dilution factor, explaining why final parasitemia can reach
750 more than 100%.
751

752 **Immunofluorescence assays and fixed fluorescence imaging**

753 Immunofluorescence assays were performed on asexual and sexual blood-stage parasites,
754 using the same fixation and staining protocols. Asexual blood-stage parasites were usually
755 synchronized with 5% sorbitol to get them in the preferred stage for imaging. For tight
756 synchronization, late-stage parasites were isolated with 63% Percoll centrifugation and

757 added to fresh RBCs. Four hours later, a 5% sorbitol was performed to select for young rings.
758 Parasites were settled on a poly-L-lysine coated coverslip for 20 min at 37°C. Parasites were
759 fixed (4% EM-grade paraformaldehyde, 0.0075% EM-grade glutaraldehyde in PBS)[58] for 20
760 min and permeabilized with 0.1% Triton X-100 for 10 min. Samples were blocked with 3%
761 bovine serum albumin (BSA) (Sigma-Aldrich) in PBS for 1 h. Primary and secondary antibody
762 incubations were performed for 1 h in 3% BSA. The nucleus was visualized by staining with 1
763 µM DAPI in PBS for 1 h. PBS washes were performed between different steps. Parasites
764 were mounted with Vectashield (Vector Laboratories). Images were taken with a Zeiss
765 LSM880 or LSM900 Airyscan microscope with 63x oil objective with 405, 488, 561, 633 nm
766 excitations. Images were Airyscan processed before analysis with FIJI software. MitoTracker
767 stainings (including MitoTracker™ Orange CMTMRos, Red CMXRos, Deep Red FM, all from
768 Thermo Fisher Scientific) were done before settling and fixation by incubation of the
769 parasites with 100 nM MitoTracker for 30 min at 37°C, followed by a wash with complete
770 media. The IMC protein GAP45 was labeled using the anti-GAP45 rabbit antibody (1:5000) (a
771 kind gift from Julian Rayner)[27] and goat anti-rabbit AlexaFluor 488 antibody (1:500,
772 Invitrogen). Alfa-tubulin was labeled with an anti-alfa tubulin mouse antibody (1:500,
773 Thermo Fisher Scientific) and chicken anti-mouse AlexaFluor 488 antibody (1:400,
774 Invitrogen). 3D visualization and quantifications were done in Arivis 4D Vision software. For
775 mitochondrial measurements, threshold-based segmentation was used. For nuclei, blob-
776 finder function was used for segmentation. Number of segmented objects and volume of
777 objects was determined automatically in Arivis software.
778
779 **Gametocyte generation and mosquito feeds**
780 Gametocyte cultures were maintained in a semi-automatic culturing system with media
781 changes twice a day[59]. MitoRed gametocytes used for imaging were induced by Albumax
782 supplementation. A mixed asexual blood-stage culture of 1% was set up and maintained in
783 medium supplemented with 2.5% Albumax II (Thermo Fisher Scientific) without human
784 serum for four days[60]. After four days, parasites were cultured in complete medium again
785 for further gametocyte development. For mosquito feeding, MitoRed gametocytes were
786 stress induced through asexual overgrowing. A mixed asexual blood-stage culture of 1% was
787 set up and maintained for 2 weeks. At day 15 after gametocyte induction, gametocytes
788 were fed to *Anopheles stephensi* mosquitoes (Sind-Kasur Nijmegen strain)[61]. 24 hours after
789 feeding, several mosquitoes were dissected, and blood bolus was obtained for live imaging
790 of ookinetes.
791
792 **Live imaging of asexual blood-stage parasites**
793 Sorbitol-synchronized MitoRed and NF54 schizonts were stained with 0.5 µg/ml Hoechst
794 33342 (Invitrogen, H3570) for 30 min at 37°C for nuclear staining. MitoTracker stainings
795 (including MitoTracker™ Orange CMTMRos, Red CMXRos, Deep Red FM, Rhodamin123, all
796 from Thermo Fisher Scientific) were done by incubation of the parasites with 100 nM
797 MitoTracker or 1 µg/ml Rhodamin123 for 30 min at 37°C, followed by a wash with complete
798 medium. Stained parasites were diluted 1:40 in complete medium and settled for 20 min at
799 37°C in a poly-L-lysine coated µ-slide 8-well imaging chamber (Ibidi). Unbound cells were
800 washed away with phenol red free complete medium in which cells were also kept during
801 imaging. Parasites were imaged on a Zeiss LSM880 Airyscan microscope with 37°C heated
802 stage table and 63x oil objective. Images were Airyscan processed before analysis with FIJI
803 software.

Live imaging of mosquito-stage parasites

Ookinetes were obtained from the blood bolus of infected mosquitoes 24 hours after feeding. Ookinetes were stained by mouse monoclonal anti-*Pf*s25 conjugated antibody (made in house, final concentration 15µg/ml). Stained sample was applied on a glass slide and covered with a glass coverslip. The sample was immediately imaged on a Zeiss LSM880 Airyscan microscope with 63x oil objective. Mosquito midguts were dissected at day 7, 10, and 13 after infection and put on a glass slide in PBS covered with a glass coverslip. Samples were imaged immediately on a Zeiss LSM880 or LSM900 microscope with 63x oil objective. Oocysts were identified based on their fluorescent mitochondrion and round shape in the brightfield channel. All images were Airyscan processed before analysis with FIJI software. 3D segmentations and visualizations were done by manual thresholding of the fluorescent signal in Arivis 4D vision software. Salivary glands were dissected on day 13, 16, and 21 after infection and stained with mouse monoclonal anti-CSP conjugated antibody (made in house, final concentration 1µg/ml). Stained glands were applied on a glass slide and covert with a glass coverslip. Samples were imaged on a Zeiss Axioscope A1 microscope with AxioCam ICc1.

FIB-SEM image analysis

FIB-SEM image stacks were reused from Evers *et al.*[20] (EMPIAR-10392). For these stacks, gametocyte-induced iGP2 parasite cultures were MACS purified. During this process many late-stage asexual parasites in these cultures were co-purified and fixed in the agarose blocks used for FIB-SEM imaging. Detailed sample preparation and FIB-SEM imaging methods are described in Evers *et al.*[20]. All image processing, visualizations and analysis was done in ORS Dragonfly software (2022.2). Segmentations were done by either manual segmentation or deep learning-based segmentation. Deep learning-based segmentations were manually reviewed and corrected when necessary. 3D renderings of segmented regions were converted to triangle meshes for visualization.

Acknowledgements

We thank members from the molecular malaria research group for the discussions. We also thank Aniek Garritsen for her contributions to the generation of the SIL plasmids. We do greatly appreciate the help from Chiara Andolina and Nicholas Proellochs with mosquito experiments. We would like to thank Astrid Pouwelsen, Jolanda Klaassen, Laura Pelser-Posthumus, Saskia Mulder and Jacqueline Kuhnen for breeding of mosquitoes and handling of the infected mosquitoes. We thank the Radboud Technology Center Microscopy, Radboud Technology Center flowcytometry, and Radboudumc Electron Microscopy Center for the use of their facilities. We are grateful to Alan Cowman for sharing the p1.2RhopH3-HA-mScarlet plasmid and Julian Rayner for sharing the anti-GAP45 antibody. J.M.J.V. is supported by an individual Radboudumc Master-PhD grant. A.B.V. is supported by an NIH grant (R01 AI028398).

845 ## References

846 1. WHO. *World malaria report 2023*. (2023).
847 2. Vaidya, A. B. & Mather, M. W. Mitochondrial evolution and functions in malaria parasites.
848 *Annu. Rev. Microbiol.* **63**, 249–267 (2009).
849 3. Painter, H. J., Morrisey, J. M., Mather, M. W. & Vaidya, A. B. Specific role of mitochondrial
850 electron transport in blood-stage Plasmodium falciparum. *Nature* **446**, 88–91 (2007).
851 4. Ke, H. *et al.* Genetic investigation of tricarboxylic acid metabolism during the Plasmodium
852 falciparum life cycle. *Cell Rep.* **11**, 164–174 (2015).
853 5. Evers, F. *et al.* Composition and stage dynamics of mitochondrial complexes in Plasmodium
854 falciparum. *Nat. Commun.* **12**, 3820 (2021).
855 6. Lamb, I. M., Okoye, I. C., Mather, M. W. & Vaidya, A. B. Unique Properties of Apicomplexan
856 Mitochondria. *Annu. Rev. Microbiol.* **77**, 541–560 (2023).
857 7. Goodman, C. D., Buchanan, H. D. & McFadden, G. I. Is the Mitochondrion a Good Malaria
858 Drug Target? *Trends Parasitol.* **33**, 185–193 (2017).
859 8. Ruiz-Trillo, I. & de Mendoza, A. Towards understanding the origin of animal development.
860 *Dev.* **147**, 1–7 (2020).
861 9. Verhoef, J. M. J., Meissner, M. & Kooij, T. W. A. Organelle dynamics in apicomplexan
862 parasites. *MBio* **12**, (2021).
863 10. van Dooren, G. G. *et al.* Development of the endoplasmic reticulum, mitochondrion and
864 apicoplast during the asexual life cycle of Plasmodium falciparum. *Mol. Microbiol.* **57**, 405–
865 419 (2005).
866 11. Rudlaff, R. M., Kraemer, S., Marshman, J. & Dvorin, J. D. Three-dimensional ultrastructure of
867 Plasmodium falciparum throughout cytokinesis. *PLoS Pathog.* **16**, e1008587 (2020).
868 12. Stanway, R. R. *et al.* Organelle segregation into Plasmodium liver stage merozoites. *Cell.*
869 *Microbiol.* **13**, 1768–1782 (2011).
870 13. Linzke, M. *et al.* Live and Let Dye: Visualizing the Cellular Compartments of the Malaria
871 Parasite Plasmodium falciparum. *Cytom. Part A* **97**, 694–705 (2020).
872 14. Painter, H. J., Morrisey, J. M. & Vaidya, A. B. Mitochondrial electron transport inhibition and
873 viability of intraerythrocytic Plasmodium falciparum. *Antimicrob. Agents Chemother.* **54**,
874 5281–5287 (2010).
875 15. Joanny, F., Held, J. & Mordmüller, B. In Vitro activity of fluorescent dyes against asexual blood
876 stages of Plasmodium falciparum. *Antimicrob. Agents Chemother.* **56**, 5982–5985 (2012).
877 16. Gebru, T., Mordmüller, B. & Heldb, J. Effect of fluorescent dyes on in vitro-differentiated,
878 late-stage plasmodium falciparum gametocytes. *Antimicrob. Agents Chemother.* **58**, 7398–
879 7404 (2014).
880 17. Matz, J. M., Goosmann, C., Matuschewski, K. & Kooij, T. W. A. An Unusual Prohibitin
881 Regulates Malaria Parasite Mitochondrial Membrane Potential. *Cell Rep.* **23**, 756–767 (2018).
882 18. Esveld, S. L. Van *et al.* A Prioritized and Validated Resource of Mitochondrial Proteins in
883 Plasmodium Identifies Unique Biology. *mSphere* **6**, e00614-21 (2021).
884 19. Kooij, T. W. A., Rauch, M. M. & Matuschewski, K. Expansion of experimental genetics
885 approaches for Plasmodium berghei with versatile transfection vectors. *Mol. Biochem.*
886 *Parasitol.* **185**, 19–26 (2012).
887 20. Evers, F. *et al.* Comparative 3D ultrastructure of Plasmodium falciparum gametocytes. *bioRxiv*
888 2023.03.10.531920 (2023).
889 21. Billker, O. *et al.* Identification of xanthurenic acid as the putative inducer of malaria
890 development in the mosquito. *Lett. to Nat.* **392**, 289–292 (1998).
891 22. Moraes, C. R. & Meyers, S. The sperm mitochondrion: Organelle of many functions. *Anim.*
892 *Reprod. Sci.* **194**, 71–80 (2018).
893 23. Vega-Rodríguez, J. *et al.* The glutathione biosynthetic pathway of Plasmodium is essential for
894 mosquito transmission. *PLoS Pathog.* **5**, 16–18 (2009).
895 24. Sturm, A., Mollard, V., Cozijnsen, A., Goodman, C. D. & McFadden, G. I. Mitochondrial ATP

896 synthase is dispensable in blood-stage Plasmodium berghei rodent malaria but essential in
897 the mosquito phase. *Proc. Natl. Acad. Sci. U. S. A.* **112**, 10216–10223 (2015).
898 25. Siciliano, G. *et al.* Critical Steps of Plasmodium falciparum Ookinete Maturation. *Front.*
899 *Microbiol.* **11**, 1–9 (2020).
900 26. Ridzuan, M. A. M. *et al.* Subcellular location, phosphorylation and assembly into the motor
901 complex of GAP45 during Plasmodium falciparum schizont development. *PLoS One* **7**, (2012).
902 27. Jones, M. L., Cottingham, C. & Rayner, J. C. Effects of calcium signaling on Plasmodium
903 falciparum erythrocyte invasion and post-translational modification of gliding-associated
904 protein 45 (PfGAP45). *Mol. Biochem. Parasitol.* **168**, 55–62 (2009).
905 28. Rudlaff, R. M., Kraemer, S., Streva, V. A. & Dvorin, J. D. An essential contractile ring protein
906 controls cell division in Plasmodium falciparum. *Nat. Commun.* **10**, 2181 (2019).
907 29. Kono, M., Prusty, D., Parkinson, J. & Gilberger, T. W. The apicomplexan inner membrane
908 complex. *Front. Biosci.* **18**, 982–992 (2013).
909 30. Voß, Y., Klaus, S., Guizetti, J. & Ganter, M. Plasmodium schizogony, a chronology of the
910 parasite's cell cycle in the blood stage. *PLoS Pathog.* **19**, 1–21 (2023).
911 31. Gerald, N., Mahajan, B. & Kumar, S. Mitosis in the human malaria parasite Plasmodium
912 falciparum. *Eukaryot. Cell* **10**, 474–482 (2011).
913 32. Liffner, B. *et al.* Atlas of Plasmodium falciparum intraerythrocytic development using
914 expansion microscopy. *Elife* 1–39 (2023) doi:10.1101/2023.03.22.533773.
915 33. Hain, A. U. P. & Bosch, J. Autophagy in Plasmodium, a multifunctional pathway? *Comput.*
916 *Struct. Biotechnol. J.* **8**, e201308002 (2013).
917 34. Ghosh, D., Walton, J. L., Roepe, P. D. & Sinai, A. P. Autophagy is a cell death mechanism in
918 Toxoplasma gondii Debasish. *Cell. Microbiol.* **23**, 1–7 (2012).
919 35. Joy, S. *et al.* Basal and starvation-induced autophagy mediates parasite survival during
920 intraerythrocytic stages of Plasmodium falciparum. *Cell Death Discov.* **4**, (2018).
921 36. Saeed, S., Tremp, A. Z., Sharma, V., Lasonder, E. & Dessens, J. T. NAD (P) transhydrogenase
922 has vital non-mitochondrial functions in malaria parasite transmission . *EMBO Rep.* **21**, 1–11
923 (2020).
924 37. Burda, P.-C. *et al.* A Plasmodium plasma membrane reporter reveals membrane dynamics by
925 live-cell microscopy. *Sci. Rep.* **7**, 9740 (2017).
926 38. Stanway, R. R., Witt, T., Zobiak, B., Aepfelbacher, M. & Heussler, V. T. GFP-targeting allows
927 visualization of the apicoplast throughout the life cycle of live malaria parasites. *Biol. cell* **101**,
928 415–430 (2009).
929 39. Roques, M., Bindschedler, A., Beyeler, R. & Heussler, V. T. Same, same but different:
930 Exploring Plasmodium cell division during liver stage development. *PLoS Pathog.* **19**, 1–22
931 (2023).
932 40. Yeh, E. & DeRisi, J. L. Chemical rescue of malaria parasites lacking an apicoplast defines
933 organelle function in blood-stage Plasmodium falciparum. *PLoS Biol.* **9**, e1001138 (2011).
934 41. Maruthi, M., Ling, L., Zhou, J. & Ke, H. Dispensable role of mitochondrial fission protein 1
935 (Fis1) in the erythrocytic development of Plasmodium falciparum. *mSphere* **5**, e00579-20
936 (2020).
937 42. Morano, A. A., Xu, W., Shadija, N., Dvorin, J. D. & Ke, H. The dynamin-related protein Dyn2 is
938 essential for both apicoplast and mitochondrial fission in. *bioRxiv* (2024).
939 43. Arnot, D. E., Ronander, E. & Bengtsson, D. C. The progression of the intra-erythrocytic cell
940 cycle of Plasmodium falciparum and the role of the centriolar plaques in asynchronous
941 mitotic division during schizogony. *Int. J. Parasitol.* **41**, 71–80 (2011).
942 44. Simon, C. S. *et al.* An extended DNA-free intranuclear compartment organizes centrosome
943 microtubules in malaria parasites. *Life Sci. Alliance* **4**, 1–15 (2021).
944 45. Striepen, B. *et al.* The plastid of Toxoplasma gondii is divided by association with the
945 centrosomes. *J. Cell Biol.* **151**, 1423–1434 (2000).
946 46. van Dooren, G. G. *et al.* A novel dynamin-related protein has been recruited for apicoplast

947 fission in Toxoplasma gondii. *Curr. Biol.* **19**, 267–276 (2009).
948 47. Vaishnava, S. *et al.* Plastid segregation and cell division in the apicomplexan parasite
949 Sarcocystis neurona. *J. Cell Sci.* **118**, 3397–3407 (2005).
950 48. Frederick, R. L. & Shaw, J. M. Moving mitochondria: Establishing distribution of an essential
951 organelle. *Traffic* **8**, 1668–1675 (2007).
952 49. Das, S., Lemgruber, L., Tay, C. L., Baum, J. & Meissner, M. Multiple essential functions of
953 Plasmodium falciparum actin-1 during malaria blood-stage development. *BMC Biol.* **15**, 1–16
954 (2017).
955 50. Periz, J. *et al.* Toxoplasma gondii F-actin forms an extensive filamentous network required for
956 material exchange and parasite maturation. *Elife* **6**, e24119 (2017).
957 51. Stortz, J. F. *et al.* Formin-2 drives polymerisation of actin filaments enabling segregation of
958 apicoplasts and cytokinesis in Plasmodium Falciparum. *Elife* **8**, 1–34 (2019).
959 52. Jacot, D., Daher, W. & Soldati-Favre, D. Toxoplasma gondii myosin F, an essential motor for
960 centrosomes positioning and apicoplast inheritance. *EMBO J.* **32**, 1702–1716 (2013).
961 53. Devarakonda, P. M., Sarmiento, V. & Heaslip, A. T. F-actin and myosin F control apicoplast
962 elongation dynamics which drive apicoplast-centrosome association in Toxoplasma gondii.
963 *MBio* **14**, (2023).
964 54. Wu, Y., Sifri, C. D., Lei, H. H., Su, X. Z. & Wellems, T. E. Transfection of Plasmodium falciparum
965 within human red blood cells. *Proc. Natl. Acad. Sci. U. S. A.* **92**, 973–977 (1995).
966 55. Crabb, B. S. & Cowman, A. F. Characterization of promoters and stable transfection by
967 homologous and nonhomologous recombination in Plasmodium falciparum. *Proc. Natl. Acad.*
968 *Sci. U. S. A.* **93**, 7289–7294 (1996).
969 56. Pasternak, M. *et al.* RhopH2 and RhopH3 export enables assembly of the RhopH complex on
970 P. falciparum-infected erythrocyte membranes. *Commun. Biol.* **5**, 1–12 (2022).
971 57. Lim, M. Y. X. *et al.* UDP-galactose and acetyl-CoA transporters as Plasmodium multidrug
972 resistance genes. *Nat. Microbiol.* **1**, (2016).
973 58. Tonkin, C. J. *et al.* Localization of organellar proteins in Plasmodium falciparum using a novel
974 set of transfection vectors and a new immunofluorescence fixation method. *Mol. Biochem.*
975 *Parasitol.* **137**, 13–21 (2004).
976 59. Ponnudurai, T., Lensen, A. H. W., Meis, J. F. G. M. & Meuwissen, J. H. E. Synchronization of
977 Plasmodium falciparum gametocytes using an automated suspension culture system.
978 *Parasitology* **93**, 263–274 (1986).
979 60. Graumans, W. *et al.* AlbuMAX supplemented media induces the formation of transmission-
980 competent P. falciparum gametocytes. *bioRxiv* 1–9 (2024).
981 61. Feldmann, A. M. & Ponnudurai, T. Selection of Anopheles stephensi for refractoriness and
982 susceptibility to Plasmodium falciparum. *Med. Vet. Entomol.* **3**, 41–52 (1989).
983